



O-3-based atomic layer deposition of hexagonal La₂O₃ films on Si(100) and Ge(100) substrates

L. Lamagna, C. Wiemer, M. Perego, S. N. Volkos, S. Baldovino, D. Tsoutsou, Sylvie Schamm-Chardon, Pierre-Eugène Coulon, M. Fanciulli

► To cite this version:

L. Lamagna, C. Wiemer, M. Perego, S. N. Volkos, S. Baldovino, et al.. O-3-based atomic layer deposition of hexagonal La₂O₃ films on Si(100) and Ge(100) substrates. *Journal of Applied Physics*, 2010, 108 (8), pp.084108. 10.1063/1.3499258 . hal-01745024

HAL Id: hal-01745024

<https://hal.science/hal-01745024>

Submitted on 9 Apr 2018

HAL is a multi-disciplinary open access archive for the deposit and dissemination of scientific research documents, whether they are published or not. The documents may come from teaching and research institutions in France or abroad, or from public or private research centers.

L'archive ouverte pluridisciplinaire **HAL**, est destinée au dépôt et à la diffusion de documents scientifiques de niveau recherche, publiés ou non, émanant des établissements d'enseignement et de recherche français ou étrangers, des laboratoires publics ou privés.

O₃-based atomic layer deposition of hexagonal La₂O₃ films on Si(100) and Ge(100) substrates

L. Lamagna, C. Wiemer, M. Perego, S. N. Volkos, S. Baldovino, D. Tsoutsou, S. Schamm-Chardon, P. E. Coulon, and M. Fanciulli

Citation: *Journal of Applied Physics* **108**, 084108 (2010); doi: 10.1063/1.3499258

View online: <https://doi.org/10.1063/1.3499258>

View Table of Contents: <http://aip.scitation.org/toc/jap/108/8>

Published by the *American Institute of Physics*

Articles you may be interested in

[La₂O₃ gate insulators prepared by atomic layer deposition: Optimal growth conditions and MgO/La₂O₃ stacks for improved metal-oxide-semiconductor characteristics](#)

Journal of Vacuum Science & Technology A: Vacuum, Surfaces, and Films **30**, 051507 (2012); 10.1116/1.4737618

[Vibrational and electrical properties of hexagonal La₂O₃ films](#)

Applied Physics Letters **91**, 102901 (2007); 10.1063/1.2779108

[Properties of lanthanum oxide thin films deposited by cyclic chemical vapor deposition using tris\(isopropyl-cyclopentadienyl\)lanthanum precursor](#)

Journal of Applied Physics **100**, 024111 (2006); 10.1063/1.2218465

[Moisture-absorption-induced permittivity deterioration and surface roughness enhancement of lanthanum oxide films on silicon](#)

Applied Physics Letters **88**, 072904 (2006); 10.1063/1.2174840

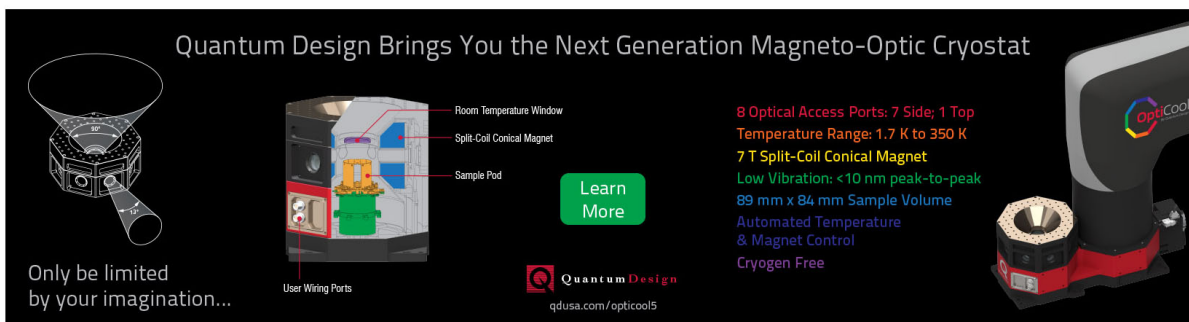
[Atomic layer deposition of lanthanum aluminum oxide nano-laminates for electrical applications](#)

Applied Physics Letters **84**, 3957 (2004); 10.1063/1.1739272

[Film properties of ALD HfO₂ and La₂O₃ gate dielectrics grown on Si with various pre-deposition treatments](#)

Journal of Vacuum Science & Technology B: Microelectronics and Nanometer Structures Processing, Measurement, and Phenomena **22**, 2121 (2004); 10.1116/1.1773840

Quantum Design Brings You the Next Generation Magneto-Optic Cryostat



The advertisement features a central cutaway diagram of the cryostat with labels: Room Temperature Window, Split-Coil Conical Magnet, Sample Pod, and User Wiring Ports. To the left is a 3D perspective view of the device. To the right is a close-up of the magnet assembly. A 'Learn More' button is positioned below the cutaway diagram.

Only be limited by your imagination...

Learn More

Quantum Design
qdusa.com/opticool5

8 Optical Access Ports: 7 Side; 1 Top
Temperature Range: 1.7 K to 350 K
7 T Split-Coil Conical Magnet
Low Vibration: <10 nm peak-to-peak
89 mm x 84 mm Sample Volume
Automated Temperature & Magnet Control
Cryogen Free

O₃-based atomic layer deposition of hexagonal La₂O₃ films on Si(100) and Ge(100) substrates

L. Lamagna,^{1,a)} C. Wiemer,¹ M. Perego,¹ S. N. Volkos,¹ S. Baldovino,² D. Tsoutsou,¹ S. Schamm-Chardon,³ P. E. Coulon,³ and M. Fanciulli^{1,2}

¹Laboratorio MDM, IMM-CNR, Via C. Olivetti 2, 20041 Agrate Brianza (MB), Italy

²Dipartimento di Scienza dei Materiali, Università degli Studi di Milano-Bicocca, 20126 Milano, Italy

³nMat group, CEMES-CNRS, Université de Toulouse, BP 94347, 31055 Toulouse cedex 4, France

(Received 29 April 2010; accepted 5 September 2010; published online 26 October 2010)

The hexagonal phase of La₂O₃ is obtained upon vacuum annealing of hydroxylated La₂O₃ films grown with atomic layer deposition at 200 °C using La(ⁱPrCp)₃ and O₃. A dielectric constant value of 24 ± 2 and 22 ± 1 is obtained on Si-based and Ge-based metal-oxide-semiconductor capacitors, respectively. However, the relatively good La₂O₃ dielectric properties are associated with significant interface reactivity on both semiconductor substrates. This leads to the identification of a minimum critical thickness that limits the scaling down of the equivalent oxide thickness of the stack. These findings are explained by the spontaneous formation of lanthanum silicate and germanate species which takes place during the growth and also upon annealing. Although the ultimate film thickness scalability remains an unsolved concern, the use of an O₃-based process is demonstrated to be a suitable solution to fabricate La₂O₃ films that can be successfully converted into the high-*k* hexagonal phase. © 2010 American Institute of Physics. [doi:10.1063/1.3499258]

I. INTRODUCTION

The transition of the complementary metal-oxide-semiconductor (CMOS) industry to the nanoelectronic era is strongly connected with the challenge to implement into sub-45 nm CMOS technology nodes novel dielectrics with a high permittivity (*k*) (i.e., high-*k* dielectrics) as alternative gate insulators in order to comply with future static power dissipation constraints.^{1,2} Indeed, major integrated circuit manufacturers have already introduced for transistor production Hf-based oxides in combination with metal gate electrodes into their 45 nm Si CMOS process line.³ Over the last few years, rare earth oxides have received extensive attention as potential gate insulators for sub-45 nm CMOS technology nodes for which an equivalent oxide thickness (EOT) below 1 nm has been envisaged.^{4,5} In particular, La₂O₃ has been identified as a promising candidate to achieve the above EOT target mainly due to its high *k* value ($k \sim 27$),^{6,7} which is achieved when the material is entirely crystallized into the hexagonal (*h*-) P6₃/*mmc* phase, and wide band gap (~ 5.3 eV).⁸ However, hygroscopicity⁹ associated to the so-called “lanthanide contraction” phenomenon⁴ impedes the acquisition of a stable *h*-La₂O₃ phase as this quickly relaxes upon air exposure to a *h*-La(OH)₃ phase^{7,10} with a concomitant *k* value degradation.¹¹ To circumvent the above issue, *in situ* La₂O₃ capping with a thin Al₂O₃ layer has been exploited in order to avoid moisture absorption but, regrettably, the *h*-La₂O₃ phase is found to be only partially promoted regardless of how the growth temperature (i.e., 260–500 °C range) and postdeposition annealing temperature (i.e., 600–1100 °C range) are chosen.¹² Differently, an ultraviolet O₃ treatment on a bare La₂O₃ surface considerably sup-

presses the moisture absorption thus preserving the *h*-La₂O₃ phase for a longer time; however, such an approach might not be fully compatible with the standard CMOS device process cycle.¹³ Other issues like the choice of the growth technique, or the development of the *h*-grains as a function of the film thickness, can further complicate the *h*-La₂O₃ phase generation. Equally important is also the fact that the “lanthanide contraction” phenomenon⁴ impairs the La₂O₃ thermal stability on Si because it gives rise, during growth and postdeposition annealing, to Si diffusion into the La₂O₃ lattice,¹⁴ therefore causing an increase in the stack EOT due to the uncontrolled formation of lanthanum silicate La_{*x*}Si_{*y*}O_{*z*} (LaSiO) interfacial layer (IL) (Ref. 15) that might be associated to an excessive defect-assisted gate leakage current.¹⁶ In general, the formation of a pure *h*-La₂O₃ phase accompanied by a minimized IL thickness still remains a serious challenge for La₂O₃/Si stacks with a few nanometers thick oxide as this tends to crystallize into the low *k* cubic (*c*-) La₂O₃ phase upon postgrowth thermal treatment.^{6,17} Concomitantly, it is widely recognized that integration of rare earth-based high-*k* dielectrics with a high carrier mobility Ge channel can pave the way for realizing sub-22 nm CMOS transistors with increased performance provided that efficient Ge surface passivation is achieved.^{18,19} In this context, a comparative study²⁰ between La₂O₃/Ge and La₂O₃/Si interfaces addressing IL thickness evolution after postdeposition annealing has revealed that the latter phenomenon is notably smaller for the Ge case than for the Si case, thus, indicating that the former interface might better serve future EOT scalability requirements than the latter one. Along these lines, a detailed investigation is mandatory in order to gain insight as to why low *k* values ($k \sim 14$ – 22) compared to the expected value ($k \sim 27$) corresponding to the pure *h*-La₂O₃ phase^{6,7} have been reported^{20–23} so far for the La₂O₃/Ge stacks. Recently, lan-

^{a)}Electronic mail: luca.lamagna@mdm.imm.cnr.it.

thanum germanate $\text{La}_x\text{Ge}_y\text{O}_z$ (LaGeO), which is almost unavoidably formed due to a strong and spontaneous reaction when La_2O_3 comes in contact with the Ge surface,²⁴ has emerged as an attractive choice for high- k /Ge interfaces because of its beneficial role in defects passivation^{24–26} and band offset enhancement.²⁷ Indeed, an intense effort within the Ge-based CMOS community is currently underway to optimize the properties of the $\text{ZrO}_2/\text{La}_2\text{O}_3$ stacks because preliminary work^{27–31} has demonstrated encouraging electrical characteristics including a large potential for stack EOT scalability below 1 nm.

La_2O_3 films have been grown on Si substrates by various techniques, namely, molecular beam deposition,^{32,33} sputtering,^{11,34} metal organic chemical vapor deposition,^{35,36} and electron beam evaporation.^{37,38} Conversely, the spread regarding the methods for La_2O_3 deposition on Ge substrates is narrower since the majority of published work is predominantly concerned with La_2O_3 growth by electron beam evaporation^{20,21} and molecular beam deposition.^{24,27–29,31} Nonetheless, it is widely acknowledged that atomic layer deposition (ALD) is the key tool to deposit innovative materials for fabricating a range of emerging nanostructures and nanodevices because it provides the capability to grow smooth and conformal films at relatively low temperatures and on large areas with an extremely accurate thickness control.³⁹ ALD growth of $\text{La}_2\text{O}_3/\text{Si}$ stacks has been routinely performed employing various precursor schemes, for example, $\text{La}(\text{thd})_3+\text{O}_3$,¹⁰ $\text{La}(\text{Cp})_3+\text{H}_2\text{O}$ or O_3 ,¹⁵ $\text{La}(\text{EtCp})_3+\text{O}_3$,⁴⁰ $\text{La}[\text{N}(\text{SiMe}_3)_2]_3+\text{H}_2\text{O}$,^{41,42} and $\text{La}(\text{PrFAMD})_3+\text{H}_2\text{O}$ or O_3 .⁴³ $\text{La}(\text{PrCp})_3$ is an interesting ALD precursor due to its relatively high vapor pressure (i.e., good volatility) stemming from the bulky alkyl group addition to the Cp ring.⁴⁴ In fact, $\text{La}(\text{PrCp})_3$ has been previously utilized in combination with H_2O for the ALD growth of $\text{La}_2\text{O}_3/\text{Si}$ stacks.⁴⁵ Recently, ALD growth by using $\text{La}(\text{PrFAMD})_3+\text{O}_2$ has also been reported³⁰ for $\text{La}_2\text{O}_3/\text{Ge}$ stacks. However, additional ALD precursor recipes should be tested in order to facilitate a broad appreciation of the ALD growth impact upon the La_2O_3 properties and $\text{La}_2\text{O}_3/\text{substrate}$ interface stability. At present, there is an increasing interest to explore O_3 instead of H_2O as the oxygen source for high- k dielectric deposition on both Si [e.g., Al_2O_3 ,⁴⁶ $\text{Hf}_x\text{Zr}_{1-x}\text{O}_2$,⁴⁷ Y-doped HfO_2 ,⁴⁸ La_2O_3 ,^{10,15,40,43} and $\text{La}_x\text{Zr}_{1-x}\text{O}_{2-\delta}$ (Ref. 49)] and Ge substrates [e.g., HfO_2 and ZrO_2 (Ref. 50) and La-doped ZrO_2 (Ref. 51)]. The difference in efficiency between the above two oxidant species in terms of reactivity, and hence oxide growth rate and quality, is accompanied by markedly diverse ALD reaction mechanisms and surface chemistries on both Si (Refs. 46 and 52) and Ge (Ref. 50) surfaces. It has been also demonstrated that O_3 might represent a valid alternative to H_2O yielding for the oxide (e.g., Al_2O_3) even better electrical properties and reliability.⁵³ It has been inferred that O_3 -based ALD of La_2O_3 , as opposed to H_2O -based one, allows to retain the self-limiting nature of the ALD reaction mechanism mitigating the formation of $\text{La}(\text{OH})_x$ species during the film growth. Moreover, it can also promote an enhanced resistance to gate leakage current associated with a high k value.^{15,43} It is worth underlying that Ge surface thermal oxidation performed in O_3 ambient at 400 °C yields a

nearly stoichiometric GeO_2/Ge interface with a comparable midgap interface trap density (D_{it}) (i.e., below $5.0 \times 10^{11} \text{ eV}^{-1} \text{ cm}^{-2}$) to state-of-the-art high- k dielectric/Si interfaces.⁵⁴ Consequently, an O_3 -based ALD recipe might be helpful in lowering the $\text{La}_2\text{O}_3/\text{Ge}$ interface defect density to an acceptable level.

We have previously demonstrated that adopting $\text{La}(\text{Cp})_3+\text{O}_3$ instead of $\text{La}(\text{Cp})_3+\text{H}_2\text{O}$ combination for the ALD of $\text{La}_2\text{O}_3/\text{Si}$ stacks notably improves interface properties through generation of a lower IL thickness and D_{it} with an expected smaller critical sample thickness for the stabilization of the $h\text{-La}_2\text{O}_3$ phase.¹⁵ In this article, we present a comparative analysis associated with the ALD of thin La_2O_3 films on both Si and Ge substrates exploiting $\text{La}(\text{PrCp})_3+\text{O}_3$ as the ALD precursor combination. Particular emphasis is devoted to the impact of the above ALD growth strategy upon the $h\text{-La}_2\text{O}_3$ phase achievement, IL formation and chemistry, $\text{La}_2\text{O}_3/\text{Si}(\text{Ge})$ interface stability, and selective electrical properties following postdeposition rapid thermal annealing (RTA). Data are also discussed and compared with those reported in the literature in order to evaluate the suitability of the proposed ALD recipe for fabricating advanced capacitors with $h\text{-La}_2\text{O}_3$ as the gate dielectric.

II. EXPERIMENTAL DETAILS

A. ALD of La_2O_3 films

Films were grown in a Savannah 200 ALD reactor (Cambridge Nanotech Inc.) on 4" H-terminated n-type Si(100) and native oxide free n-type Ge(100) wafers. The H-terminated Si(100) was obtained after Radio Corporation of America cleaning ($\text{HCl}:\text{H}_2\text{O}_2:\text{H}_2\text{O}=1:1:5$, 10 min at 85 °C) and a 30 s dip in a diluted HF solution ($\text{HF}:\text{H}_2\text{O}=1:50$, at room temperature), both followed by a 30 s rinse in deionized water. Removal of native GeO_2 was achieved with a 30 s dip in a diluted HF solution ($\text{HF}:\text{H}_2\text{O}=1:25$), at room temperature, followed by a 30 s rinse in deionized water. La_2O_3 films were deposited at a growth temperature of 200 °C alternating pulses of $\text{La}(\text{PrCp})_3$ and O_3 ; the layers thickness was tuned varying the number of ALD cycles. ALD cycle structure was composed of 15 s $\text{La}(\text{PrCp})_3$ pulse/8 s purge with $\text{N}_2/0.015 \text{ s O}_3$ pulse/6 s purge with N_2 . La source (supplied by SAFC Hitech) was kept at 150 °C; O_3 was obtained starting from ultra pure O_2 and was injected into the reactor at a concentration of $\sim 200 \text{ g/N m}^3$. One film (i.e., sample S7_ H_2O) was deposited using, for the second half of the ALD cycle, 0.015 s H_2O pulse/8 s purge with N_2 . Film thickness was estimated by spectroscopic ellipsometry (SE) using an M2000-F (J.A. Woollam Co., Inc.). A linear relationship between the film thickness and the number of ALD cycle was achieved; steady-state growth rate of La_2O_3 films was $\sim 1.0 \pm 0.1 \text{ Å/cycle}$. In Table I, the list and the total thickness of the as-grown and annealed samples discussed in the paper are reported.

B. Characterization and MOS preparation

The structural, compositional, electrical properties of the as-grown and annealed La_2O_3 films were characterized by means of: (i) grazing incidence X-ray diffraction (GIXRD),

TABLE I. Total thickness (measured by SE) and postdeposition annealing details of the as-grown and annealed samples discussed in this work.

Sample	Stack	Thickness as-grown (nm)	RTA in vacuum (°C)	Thickness after RTA (nm)
S1	<i>n</i> -Si/La ₂ O ₃	41.0	600	36.0
S2	<i>n</i> -Si/La ₂ O ₃	34.9	600	30.0
S3	<i>n</i> -Si/La ₂ O ₃	30.3	600	24.7
S4	<i>n</i> -Si/La ₂ O ₃	22.1	600	19.7
S5	<i>n</i> -Si/La ₂ O ₃	10.5	600	10.4
S6	<i>n</i> -Si/La ₂ O ₃	4.6	600	5.4
S7_H ₂ O	<i>n</i> -Si/La ₂ O ₃	~38
G1	<i>n</i> -Ge/La ₂ O ₃	20.4	400	14.6
G2	<i>n</i> -Ge/La ₂ O ₃	14.8	400	9.1
G3	<i>n</i> -Ge/La ₂ O ₃	10.0	400	6.8
G4	<i>n</i> -Ge/La ₂ O ₃	5.6	400	3.8

(ii) X-ray reflectivity (XRR), (iii) high resolution transmission electron microscopy (HRTEM), (iv) time of flight secondary ion mass spectroscopy (ToF SIMS), (v) capacitance-voltage (*C-V*), and conductance-voltage (*GV*) measurements. The postdeposition RTA was performed at 600 °C in vacuum (~1 mbar) for 60 s using a Jet First (Jipelec). GIXRD and XRR were performed as described elsewhere.⁵⁵ HRTEM was performed with the [110] direction of the Si and Ge substrates parallel to the electron beam, details are presented in Ref. 15. ToF SIMS depth profiles were acquired in negative polarity on an ION-TOF IV instrument using Cs⁺ ions at 1 keV for sputtering and Ga⁺ ions at 25 keV for analysis. *C-V* and *GV* measurements were performed exclusively on annealed stacks at room temperature with the aid of MOS capacitors patterned with Al gates (dot area ~0.85 × 10⁻⁵ cm²) fabricated by thermal evaporation through a shadow mask. To avoid moisture absorption, MOS devices were mounted inside a cryomanipulator system operated in vacuum immediately after the metallization process. Capacitance equivalent oxide thickness (CET) was determined from the device accumulation capacitance at 100 kHz.

III. LA₂O₃ FILMS ON SI(100)

A. Structural and chemical properties

GIXRD analysis is performed on both as-grown and annealed La₂O₃ films in order to address the evolution of the crystallographic structure. Figure 1 illustrates GIXRD analysis performed on sample S4 (22.1 nm, as-grown) and reveals that as-grown films deposited on Si(100) are mainly amorphous. The powder patterns of hexagonal La(OH)₃ (Ref. 56) and hexagonal La₂O₃ (Ref. 57) are added for comparison. A large bump centered at the position of the main peaks belonging to the hexagonal La(OH)₃ phase is identified in the as-deposited state. This finding confirms that, although the measurement was performed immediately after the film deposition, as expected La₂O₃ films grown by ALD are chemically unstable in air and prone to moisture absorption. Given the proved fast conversion to La(OH)₃ upon air exposure, we have decided not to investigate the electrical prop-

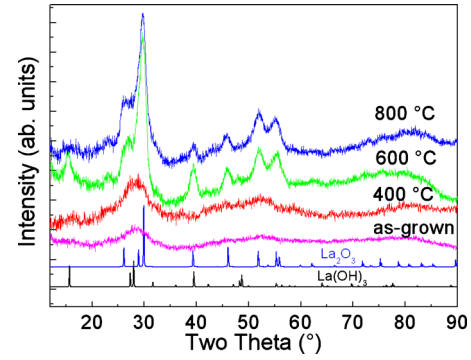


FIG. 1. (Color online) GIXRD spectra acquired for as-grown and annealed in vacuum (400, 600, and 800 °C) ~20 nm thick films (sample S4) deposited on Si(100). Hexagonal La(OH)₃ and hexagonal La₂O₃ patterns are added for comparison.

erties of as-grown films. We had previously reported, for samples deposited using a different ALD precursors combination, that a postdeposition RTA performed in vacuum (~1 mbar) promotes the crystallization of the as-grown films into the *h*-La₂O₃ phase.^{6,7,11} In light of this observation, we have decided to systematically investigate the effect of this specific thermal treatment and the related evolution of the crystallographic structure of the La₂O₃ samples grown using an O₃-based ALD process. The GIXRD spectra of the films annealed at 400, 600, and 800 °C (i.e., sample S4) are shown in Fig. 1. It is worth noticing that RTA performed at 400 °C already modifies the crystallographic order of the film although, in this case, a full crystallization is not accomplished. Indeed, because of the fairly low thermal budget, the removal of OH groups from the hydroxide layer may not be sufficient to allow a complete structural conversion. In contrast with what was observed in films grown using the La(Cp)₃+H₂O ALD recipe, in the 300–500 °C annealing temperature range we do not observe the formation of the *c*-La₂O₃ phase.⁷ On the other hand, this study confirms our previous finding⁶ that annealing at 600 °C promotes an almost complete conversion of the amorphous and partially hydroxylated layer into crystalline *h*-La₂O₃. The lattice parameters extracted from Rietveld refinement are *a* = 3.92 ± 0.01 Å and *c* = 6.19 ± 0.01 Å, in fairly good agreement with those reported for hexagonal La₂O₃ (*a* = 3.94 Å and *c* = 6.13 Å).⁵⁷ Further increase in the annealing temperature up to 800 °C does not seem to significantly affect the crystallization of the layer. It should be noted that also the crystallized *h*-La₂O₃ films obtained with the O₃-based ALD recipe completely relaxes to La(OH)₃ when exposed to air. Similar GIXRD analysis (data not shown) on La₂O₃ films thinner than 20 nm (e.g., samples S5 and S6) reveals that it is not possible to achieve crystallinity into the *h*-La₂O₃ phase across most of the sample thickness extent. This finding, which can be correlated with RTA-induced Si diffusion from the substrate into the overlayer, will be addressed in a forthcoming part of this section.

The electron density (ρ) profiles extracted from the simulation of the XRR data acquired on sample S4 are shown in Fig. 2. The ρ values reported for *h*-La₂O₃ and for the crystallized hydroxides are also reported for comparison; the profiles are superimposed at the Si(100) interface. After

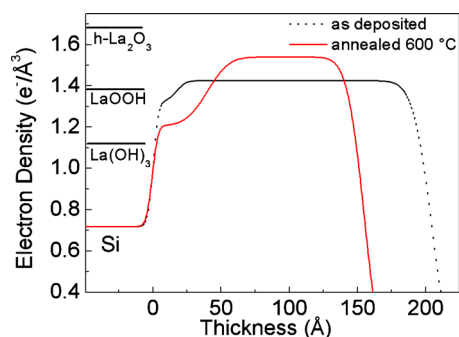


FIG. 2. (Color online) Electron density profiles extracted from the simulation of XRR data for as-grown (dotted line) and annealed in vacuum at 600 °C (continuous line) ~ 20 nm thick films deposited on Si(100) (sample S4).

annealing at 600 °C, the ρ of the layer increases together with a corresponding thickness reduction. Therefore, the densification of the layer due to both OH desorption and crystallization processes is confirmed. Upon annealing, main modifications are found to occur also at the interface with Si(100), with the formation of a wider interfacial region that is characterized by a crescent-shaped ρ profile.

Additional structural information at the $\text{La}_2\text{O}_3/\text{Si}$ interface is provided, with nanometric-scale resolution, by HRTEM analysis. Figure 3 displays a HRTEM image for a ~ 20 nm thick La_2O_3 film (i.e., sample S4) before (a) and after (b) RTA at 600 °C. An amorphous transition region between the Si substrate and the film, corresponding to an IL formed during the ALD growth, is approximately indicated by the white dotted lines. The thickness of the IL increases with annealing from about ~ 1.5 nm up to a value of ~ 5 nm. These results are in agreement with the XRR findings of an interfacial region that becomes wider upon thermal treatment. It is worth noticing that the thickness of such an IL, either before or after RTA, is confirmed to be minimized in extension if compared with those observed in La_2O_3 films grown on H-terminated Si(100) using H_2O as oxygen source.¹⁵ However, after the amorphous IL it is possible to identify a region containing nanometer-sized crystals already in the as-grown film; much more large crystals are present in the annealed film. The latter finding manifests, in accordance with the GIXRD data shown in Fig. 1, that RTA process at 600 °C induces an almost complete crystallization of the film.

In order to address the evolution of the chemical composition at the $\text{La}_2\text{O}_3/\text{Si}$ interface and within the La_2O_3

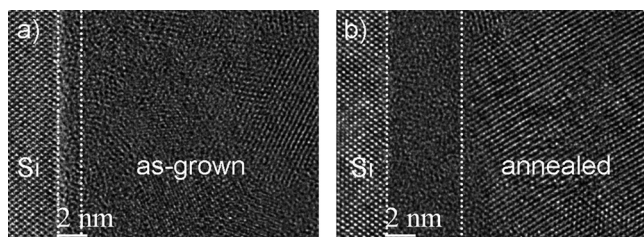


FIG. 3. HRTEM cross sections of ~ 20 nm thick (a) as-grown and (b) annealed $\text{La}_2\text{O}_3/\text{Si}$ stacks (sample S4). Dotted white lines are a guide for the eyes to visualize the borderline between the amorphous and the crystalline parts of the film.

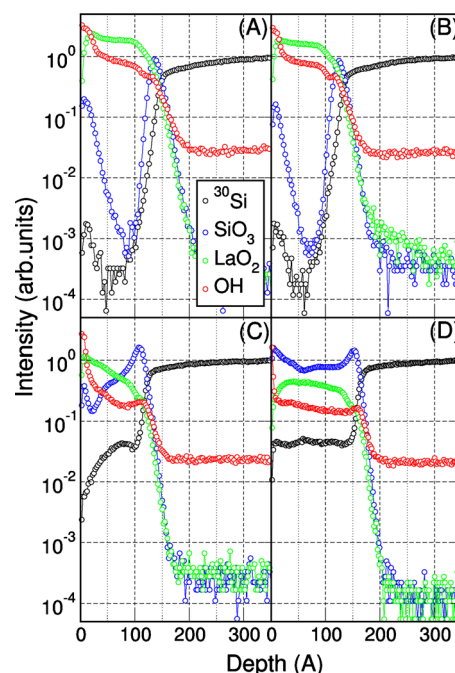


FIG. 4. (Color online) ToF SIMS depth profiles acquired on ~ 10 nm thick films deposited on Si(100) (sample S5); as-grown (a) and annealed in vacuum at 400 °C (b), 600 °C (c), and 800 °C (d).

films, ToF SIMS depth profiles were acquired on ~ 10 nm thick La_2O_3 film (i.e., sample S5) in the as-grown state and after annealing. In Fig. 4, the ToF SIMS profiles of as-grown sample (A) are compared with those acquired after RTA performed in vacuum at 400 °C (B), 600 °C (C) and 800 °C (D). In good agreement with the HRTEM findings, the presence of an IL in the as-grown sample is revealed by monitoring the SiO_3 peak, as displayed in Fig. 4(a), thus suggesting the presence of a SiO_x -like component which coexists with the La-based profile (i.e., LaO_2) in the region at the film/substrate interface. In addition, in the as-grown film, the SiO_3 and ^{30}Si signals detected at the surface reveal a moderate Si diffusion occurring through the La_2O_3 film during the ALD growth. Finally, the depth profile of the OH signal in Fig. 4(a) confirms the results of the GIXRD data analysis further attesting the marked hygroscopicity of the as-grown La_2O_3 films. The analysis of the ToF SIMS depth profiles after the 400 °C thermal treatment [Fig. 4(b)] reveals that the chemical composition of the film has not been significantly affected by such a relatively low temperature annealing process. Indeed, the IL seems stable in terms of thickness and composition and the Si distribution throughout the layer does not appear modified. Interestingly, despite the annealing process is performed in vacuum, the OH profile is slightly altered, in good agreement with the GIXRD results. No significant modifications in the structure of the layer are revealed, thus confirming that a full $\text{La}(\text{OH})_3$ conversion cannot be accomplished at an annealing temperature of 400 °C. In Fig. 4(c), the depth profiles of the sample annealed at 600 °C are reported. A clear reduction in the intensity of the OH signal is observed, in accordance with the structural analysis, hence supporting the hypothesis of the $\text{La}(\text{OH})_3$ conversion into $h\text{-La}_2\text{O}_3$ upon annealing at 600 °C. The ^{30}Si signal indicates that Si atoms diffusion, from the substrate

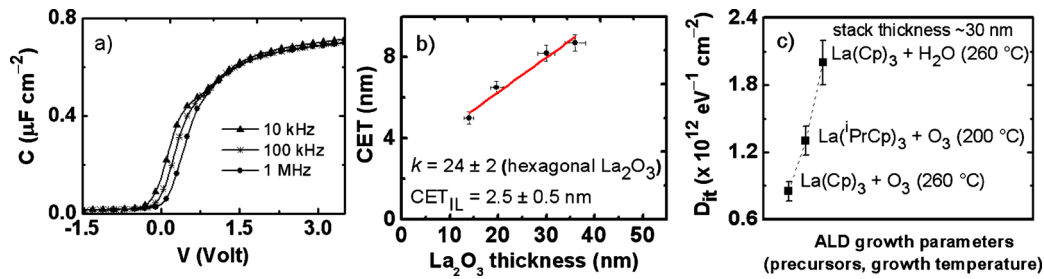


FIG. 5. (Color online) (a) C - V curves for Si-based MOS capacitors including ~ 20 nm of La_2O_3 annealed at 600 °C in vacuum (sample S4). (b) CET plot vs La_2O_3 physical thickness (c) Comparison between D_{it} values obtained on La_2O_3 /Si stacks prepared with different ALD recipes.

through the film, occurred during the thermal treatment. According to all the above results, the stack order atop the Si substrate after RTA at 600 °C can be roughly approximated by a trilayer structure composed by an amorphous IL (most likely LaSiO species), a crystalline layer characterized by a decreasing Si content and a very thin $\text{La}(\text{OH})_3$ surface layer. The presence of such a thin $\text{La}(\text{OH})_3$ capping layer might be explained either by a not complete removal of the hydroxide component during the thermal treatment or by a rehydroxylation occurred during exposure to air before the ToF SIMS measurements. When the annealing temperature is increased up to 800 °C [Fig. 4(d)], the thin $\text{La}(\text{OH})_3$ layer vanishes and no further reduction in the OH signal intensity is detected. Moreover, the ^{30}Si signal in Fig. 4(d) assumes a flat profile along the whole stack thickness indicating that, with a high temperature thermal treatment, Si diffusion from the substrate throughout the entire stack thickness is promoted. However, this finding does not imply that the whole layer should be considered fully converted into LaSiO species. Indeed, the layer is most likely composed by a mixture of hexagonal La_2O_3 and LaSiO phases or could present Si atoms at the grain borders of the crystalline hexagonal La_2O_3 . It is important to note that from GIXRD measurements we do not detect the formation of crystalline LaSiO phases.

B. Electrical properties

Figure 5(a) illustrates multifrequency C - V curves obtained for the sample S4 annealed in vacuum at 600 °C. Accumulation capacitance exhibits minor frequency dispersion within the 10–1000 kHz range. From the slope of a linear fit to a CET versus La_2O_3 thickness plot shown in Fig. 5(b), the k value for the annealed La_2O_3 films is calculated to be 24 ± 2 . According to the structural analysis, La_2O_3 thickness is calculated by using the stack thickness corrected with a 5 nm thick IL; such an IL was considered independent on the total film thickness. The presence of the ultrathin $\text{La}(\text{OH})_3$ capping layer, as detected by ToF SIMS analysis, was neglected. Annealed samples taken under consideration in the CET plot of Fig. 5(b) are S1, S2, S3, and S4. In agreement with our GIXRD data, the extracted k value conclusively confirms that RTA at 600 °C in vacuum induces film crystallization into the h - La_2O_3 phase. It is noted that the lowest boundary associated with the k value derived here for the h -phase falls outside the typical range cited in the literature,^{6,7} thus, suggesting a possible coexistence of the crystalline part with an amorphous silica-based phase which

is affecting the dielectric response of the whole stack. The fit in Fig. 5(b) intercepts with the y-axis at a point corresponding to an IL with a CET of about 2.5 ± 0.5 nm which, in turn, yields, assuming the k value for the IL to be ~ 11 (Ref. 15) an IL physical thickness of around 6–8 nm. This finding is in line with both HRTEM and ToF SIMS results, acquired on the sample annealed at 600 °C, where a significant Si diffusion, associated with the formation of LaSiO species, has been evidenced through about half (~ 5 nm) of the approximately 10 nm thick stack. An actual high k , which gradually points to the expected value of 27, could be probably obtained via increasing the total thickness of the electrical samples. The electrical analysis has been limited to the samples in which the structure, after annealing, can be mainly considered h - La_2O_3 and in which the interfacial region constitutes only a reasonably small part of the whole stack. On the contrary, in very thin films (< 10 nm; e.g., samples S5 and S6) the k value would probably point to a value typical for LaSiO (~ 11) rather than to the one associated to the h -phase. However, it is worth considering that the electrical analysis performed on the samples grown using the O_3 -based ALD recipe discussed in this work reveals the possibility to obtain h - La_2O_3 for a reduced stack thickness than the ones we have previously reported.^{6,7,15} This finding is associated to the obtainment of a less extended LaSiO region at the interface by means of the use of O_3 and probably also of a lower growth temperature. The restraintment of the interfacial LaSiO region permits the crystallization of a more extended part of the film into h - La_2O_3 and consequently the scaling down of the total EOT. Figure 5(c) displays the average D_{it} , as derived from loss peak of the GV curve at 100 kHz (Hill–Coleman method⁵⁸), for three La_2O_3 -based stacks which are of similar thickness (~ 30 nm) prepared on Si(100) using different combinations of ALD precursors, namely, (i) $\text{La}(\text{Cp})_3 + \text{H}_2\text{O}$,⁶ (ii) $\text{La}(\text{Cp})_3 + \text{O}_3$,¹⁵ and (iii) $\text{La}(\text{PrCp})_3 + \text{O}_3$ (this work). Although the ALD precursor scheme tested in this study is very effective in stabilizing the h - La_2O_3 phase at a smaller sample thickness compared to the cases in Ref. 15, it generates, as manifested through the C - V stretch out and frequency-dependent hump in Fig. 5(a), a sizable D_{it} which must be further reduced in order to fulfill advanced gate stack technology requirements.

As far as the D_{it} is concerned, in this work we confirm the trend proposed in Ref. 15 that O_3 turns out to be a better oxygen precursor choice than H_2O . Nevertheless, because of the different growth temperatures employed in the various ALD processes, it is not possible to make a direct comparison

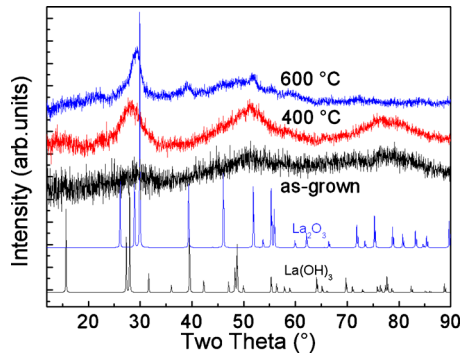


FIG. 6. (Color online) GIXRD spectra acquired for as-grown and annealed in vacuum (400 and 600 °C) ~ 20 nm thick films (sample G1) deposited on Ge(100). Hexagonal $\text{La}(\text{OH})_3$ and hexagonal La_2O_3 patterns are added for comparison.

son between the two lowest D_{it} values obtained using the two O_3 -based ALD recipes. We should also bear in mind that an increase in growth temperature plays a key role in determining the oxide/semiconductor interface electrical quality and therefore the D_{it} .

IV. La_2O_3 FILMS ON GE(100)

A. Structural and chemical properties

We analyze by means of GIXRD the crystallographic ordering of La_2O_3 as-grown and annealed films, deposited using the O_3 -based ALD recipe on native oxide free Ge(100). The measurements were performed immediately after the growth or the annealing treatment in order to minimize the effect of air exposure. The powder patterns of hexagonal $\text{La}(\text{OH})_3$ (Ref. 56) and La_2O_3 (Ref. 57) are added for comparison with the spectra acquired for the sample G1. No clear evidence of crystallographic ordering is found in the as-grown film (Fig. 6), the latter result is attributed to the absence of long range order due to the mixture of La-based hydroxides. Differently, a single broad peak in the two theta $\sim 29^\circ$ region is visible after RTA at 400 °C. The two theta position of this peak corresponds to the increase in the long range order. Annealing at 600 °C promotes a more pronounced crystallization of the La_2O_3 in its *h*-phase. The lattice parameters extracted from the Rietveld refinement of the GIXRD data are $a = 3.96 \pm 0.01$ Å and $c = 6.26 \pm 0.01$ Å, slightly higher than those obtained for the films deposited using the same ALD recipe on Si(100) and annealed at the same temperature.

The ρ profiles, extracted by simulating the XRR curves of as-grown and 400 °C annealed samples (Fig. 7), support the fact that the as-grown layers are mainly composed by La hydroxides formed by the incorporation of OH groups upon air exposure. Profiles are superimposed at the Ge(100) interface. Upon RTA performed at 400 °C in vacuum, the density of the La-based layer is found to increase up to a value which approaches the one reported for *h*- La_2O_3 . For the as-grown state (Fig. 7, dotted line), XRR reveals a decrease in the ρ close to the interface with Ge(100) that might be related to the formation of a less dense interfacial region. Differently, the value of the ρ extracted after annealing (Fig. 7, continuous line) appears uniform along the whole film thickness.

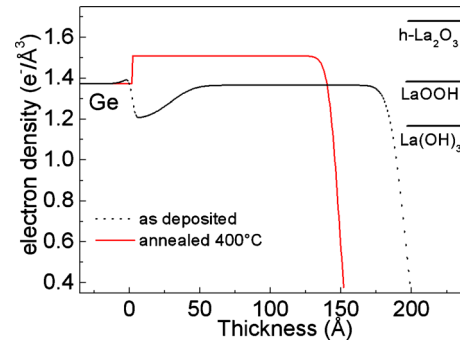


FIG. 7. (Color online) Electron density profiles extracted from the simulation of XRR data for as-grown (dotted line) and annealed in vacuum at 400 °C (continuous line) ~ 20 nm thick film deposited on Ge(100) (sample G1).

This finding might be tentatively explained with the hypothesis that the ρ of the LaGeO species, that is likely forming at the $\text{La}_2\text{O}_3/\text{Ge}$ interface upon annealing, is similar to the ρ of the *h*- La_2O_3 polymorph. Indeed, the ρ values reported for crystallized lanthanum germanates vary in the $1.38\text{--}1.45$ $\text{e}^-/\text{\AA}^3$ range. Therefore, differently than for the films deposited on H-terminated Si(100), from the ρ profiles it is not possible to clearly define the extension of the interfacial region.

Additional structural information with nanometric-scale resolution is provided for both as-grown and annealed La_2O_3 films by HRTEM analysis. Figure 8 shows HRTEM images of La_2O_3 film (i.e., sample G3) deposited on Ge(100). In the as-grown film [Fig. 8(a)] there is no evidence of a “structural” amorphous IL, despite an O_3 -based ALD process might be expected to promote an oxidation of the Ge(100) cleaned surface during the deposition.⁵⁹ Moreover, after RTA from the HRTEM cross section shown in Fig. 8(b) it is not possible to identify an amorphous structural IL atop the Ge(100). Nanocrystals can be identified within the film in both cases. However, the presence of the nanocrystals is more evident after annealing, in agreement with an increase in the crystalline order suggested by GIXRD analysis. The HRTEM findings hence support the conclusions of the structural characterization; there is no evidence of the formation of an IL during O_3 -based growth and the film/substrate interface looks sharp even after RTA.

In order to assess the chemical composition within the film and at the interface with Ge(100), ToF SIMS depth profiles were acquired on sample G2 in the as-grown state and

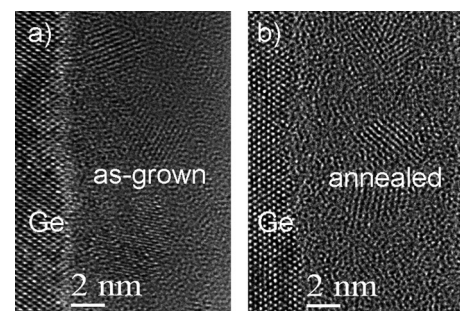


FIG. 8. HRTEM cross sections of ~ 10 nm thick (a) as-grown and (b) annealed at 400 °C in vacuum $\text{La}_2\text{O}_3/\text{Ge}$ stacks (sample G3).

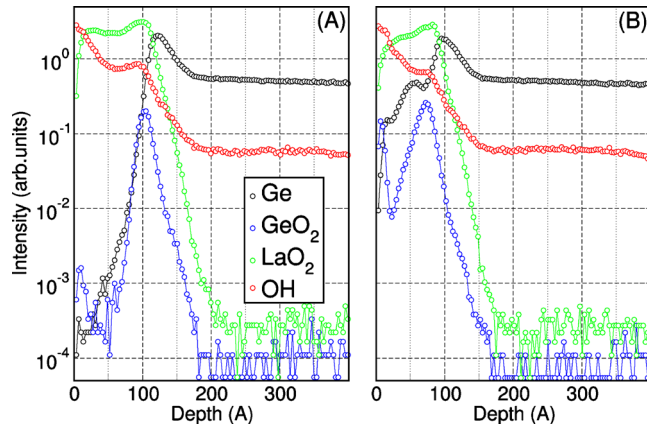


FIG. 9. (Color online) ToF SIMS depth profiles acquired on ~ 15 nm thick (sample G2) as-grown (a) and annealed at 400°C (b) films deposited on Ge(100).

after annealing at 400°C . In Fig. 9(a), the intense GeO_2 signal at the $\text{La}_2\text{O}_3/\text{Ge}$ interface indicates the presence of a Ge-rich interfacial region already in the as-grown sample. Given the aforementioned XRR and HRTEM results, such a GeO_2 signal can be attributed to the presence of a dense lanthanum germanate region of undefined thickness extension. Therefore, ToF SIMS indicates the presence of a so-called “chemical” IL as already observed for La-doped ZrO_2 films deposited on Ge(100).⁵¹ No intense Ge related signals are detected at the surface of the La_2O_3 film, suggesting a limited Ge diffusion during ALD growth. As expected, in the as-grown state the shape of the OH profile unveils the presence of a relevant hydroxide component in the film. After annealing at 400°C [Fig. 9(b)], the OH profile is only slightly modified. As already demonstrated for the $\text{La}_2\text{O}_3/\text{Si}$ stack, such low thermal budget is not sufficient to promote the complete removal of the $\text{La}(\text{OH})_3$ component. The Ge and GeO_2 signals appear more extended into the layer indicating that Ge diffusion has occurred during RTA. The graded Ge profile detected inside the La_2O_3 layer results in a not uniform Ge distribution along the thickness of the film. Therefore, atop a chemical IL composed mainly by LaGeO_3 , the $h\text{-La}_2\text{O}_3$ nanocrystals coexist with a graded Ge profile through the film; Ge atoms could be located at the grain borders. We believe that the use of a higher postdeposition annealing temperature or of a longer annealing time, would probably promote a further diffusion of Ge through the whole film thickness.

B. Electrical properties

C-V characteristics acquired for sample G1 are shown in Fig. 10(a). The hysteresis corresponds to trapped positive charges, probably related to the incomplete OH desorption or to the not optimal saturation of the defects at or close to the interface with Ge. From the CET versus La_2O_3 thickness plot [Fig. 10(b)], a k value of 22 ± 1 is calculated for the set of annealed films (i.e., samples G1, G2, and G3). This value is in line with the highest boundary reported in literature for the range of k values associated to $h\text{-La}_2\text{O}_3$ on Ge(100). Although slightly smaller, the k value appears to be in fairly good agreement with the one calculated for the same films deposited on Si(100). The difference could be associated to a more efficient conversion of the hydroxide layer into $h\text{-La}_2\text{O}_3$ phase occurring in the $\text{La}_2\text{O}_3/\text{Si}$ stacks annealed at 600°C . Moreover, in these Ge-based stacks the identification of a clear IL is extremely complex. The k value was extracted reasonably assuming a 2 nm thick IL and thus calculating the resulting La_2O_3 thickness. The extraction of the dielectric constant is not affected by this assumption. On the contrary, the discussion of the CET intercepts ($\sim 2.4 \pm 0.5$ nm assuming the IL thickness at 2 nm) with the y-axis must be addressed with particular care because of the uncertainties on the thickness and k of the IL that are likely to be modified upon RTA. We are prone to believe, also referring to the literature reports about $\text{La}_2\text{O}_3/\text{Ge}$ stacks, that also in our system a lanthanum germanate compound ($k \sim 5\text{--}6$) should be present at the interface. Therefore, the actual thickness of the “chemical” IL could be larger than 2 nm. Nevertheless, in order to address this specific issue a more detailed chemical investigation of the interface composition is needed⁶⁰ as extensively discussed in Ref. 51. The D_{it} should be extracted at high frequency, and thus at more positive voltages, in order to be in the depletion regime. However, values extracted at lower frequency could yield to an overestimation of the D_{it} since in the weak inversion regime also the minority carriers contribute to the conductance mechanisms. For this reason, D_{it} values were evaluated with the Hill-Coleman method⁵⁸ at 500 kHz. The D_{it} is found to be $\sim 3.5 \times 10^{12} \text{ eV}^{-1} \text{ cm}^{-2}$, independently of the film thickness. D_{it} values obtained for the annealed samples considered in this work are compared, in Fig. 10(c), to data reported in literature for annealed $\text{La}_2\text{O}_3/\text{Ge}$ stacks. It is worth noticing that, with the present work, we confirm the trend that the use of O_3 (Ref. 54) associated to the presence of La at the interface^{29,51} turns out to be helpful in keeping the D_{it} value

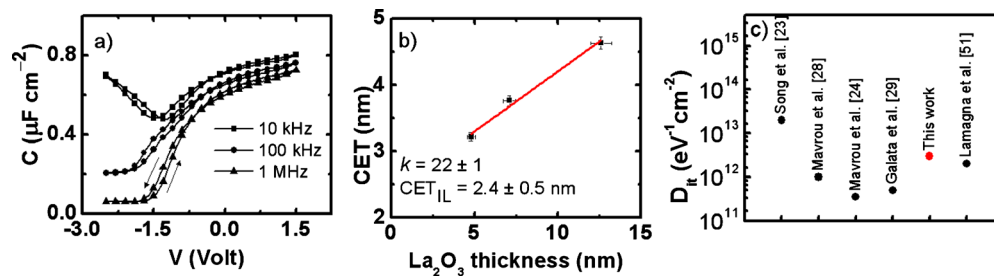


FIG. 10. (Color online) (a) C-V curves for Ge-based MOS capacitors including ~ 15 nm of La_2O_3 annealed at 400°C in vacuum (sample G1). (b) CET plot vs La_2O_3 physical thickness. (c) Comparison between D_{it} values obtained on $\text{La}_2\text{O}_3/\text{Ge}$ stacks prepared with different growth techniques.

relatively low due to the formation of LaGeO species.^{26,28} Because of the different growth temperatures and postdeposition annealing treatments employed in the different papers, it is not possible to make a direct comparison between the D_{it} values. However, it is worth considering that Song *et al.*^{21,23} reported that, with vacuum annealing, it is possible to obtain a larger stack capacitance although associated with higher D_{it} values. This observation is in line with our discussion about the efficiency of the vacuum annealing treatment in promoting, with a better efficiency, the formation of the h -La₂O₃ phase. The lowest D_{it} value presented in Fig. 10(c) was indeed associated in Ref. 24 to the use of high deposition temperature (360 °C) combined to the use of a postdeposition annealing in H₂ ambient. This might explain the fact that films discussed in this work, grown by ALD at 200 °C, present a comparatively higher D_{it} value as also revealed in the case of samples grown on Si(100).

V. DISCUSSION: SI- AND GE-BASED STACKS

The formation of h -La₂O₃ phase upon RTA in vacuum of La₂O₃ films grown by ALD has been investigated in two different oxide/semiconductor stacks. From our study and from the comparison with literature results, it turns out that the stabilization of such a high permittivity phase actually depends on three main factors which are discussed and summarized in the following Secs. V A–V C.

A. ALD precursors

The structure of the as-grown La₂O₃ films is determined not only by the growth temperature, as expected, but also by the choice of the ALD precursors (i.e., La and O source). Indeed, in general as-grown La₂O₃ films may consist of a mixture in which an amorphous hydroxide part, formed during the H₂O-based ALD process and/or upon exposure to air, coexists with a small amount of crystalline La(OH)₃ and/or c -La₂O₃. The presence of the latter phase, which is characterized by a lower k value ~ 17 and therefore undesired, depends on the ALD recipe employed and was reported either for H₂O- (Refs. 7 and 41) or for O₃-based growths.¹⁰ Therefore, how the different crystalline structures are generated should be discussed also referring to the key role played by the La source in determining either the reactivity of the ALD process or the C and H impurities content in the film.⁶¹ The presence of La(OH)₃ and/or c -La₂O₃ in the as-grown film affects and conditions the development of the hexagonal La₂O₃ polymorph during the postdeposition annealing. The use of La(¹PrCp)₃, at a growth temperature of 200 °C and in combination with O₃, leads to the obtaining of almost fully amorphous layers. As-grown films convert into La(OH)₃ upon air exposure while there is no evidence of the presence of the c -La₂O₃ phase. Subjected to RTA in vacuum these films can be transformed into h -La₂O₃ as it has been demonstrated by GIXRD analysis and by the electrical characterization.

On the other hand, for the deposition of an extremely hygroscopic compound, the selection of the oxygen source appears to be even more critical. Figure 11(a) displays the ToF SIMS depth profiles acquired for the sample S7_H₂O

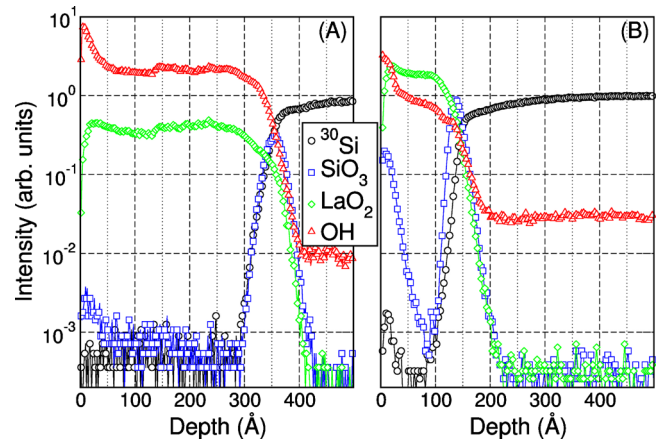


FIG. 11. (Color online) ToF SIMS chemical depth profiles acquired on (a) ~ 38 nm thick as-grown film deposited using the H₂O-based ALD recipe (sample S7_H₂O) and (b) ~ 10 nm thick as-grown film deposited using O₃-based ALD recipe (sample S5).

(as-grown, ~ 38 nm), deposited using the H₂O-based ALD recipe while in Fig. 11(b) the signals related to the sample S5 (as-grown, ~ 10 nm) deposited using O₃ are plotted. OH and LaO₂ profiles are markedly different in the two cases. The film grown using H₂O as oxygen source presents a relatively low LaO₂ signal accompanied by a very intense OH emission. Moreover the sample is characterized by an almost uniform OH distribution along the whole film thickness thus suggesting a complete hydroxylation occurred directly during ALD and related to the continue exposure to a H₂O rich ambient. Differently, the film deposited using O₃ presents a high LaO₂ signal and low OH secondary ion emission. The different intensity of the LaO₂ signal in the two samples is undoubtedly related to a variation in the film composition. O₃ provides a clear improvement in reducing the undesired incorporation of OH that may occur during the growth thus disturbing the pure ALD behavior and promoting chemical vapor deposition side-reactions.⁴³ Finally, the selection of the oxygen source strongly affects diffusion mechanism at the oxide/semiconductor interface during the film growth. Different ³⁰Si and SiO₃ signals are detected in the two cases providing indication of a Si out-diffusion and segregation at the oxide surface in the film grown using O₃ as oxygen precursor. Considering that the films were grown at the same temperature, we can explain this experimental evidence as a consequence of the obtaining of two clearly distinct films from the chemical viewpoint.

B. Postdeposition thermal treatment

The results presented in this work confirm that the postdeposition thermal treatment must be properly selected while addressing the final properties of the annealed oxide. Indeed, the use of vacuum annealing technology (~ 1 mbar) plays a crucial role in reducing the OH content and removing the undesired hydroxide component from the La₂O₃ layers.^{6,8} However, due to a fairly insufficient removal of the OH groups, only a limited increase in the long range order can be promoted in films annealed at 400 °C.^{7,62} Actually, the crystallization into the h -polymorph is accomplished when the thermal treatment is performed in vacuum and concurrently

the annealing temperature is 600 °C, thus considerably removing the hydroxide and hence promoting the phase transformation. It is noted that a relevant chemical reaction at the La_2O_3 /substrate interface is induced by such a postdeposition annealing. Nevertheless, in order to preserve the high k value obtained upon vacuum annealing, an ultimate compatible device process flow should be implemented and refined in order to completely solve the serious hygroscopicity issue related to the use of h - La_2O_3 films in an actual industrial process.

C. Si and Ge diffusion: Formation of LaSiO and LaGeO species

As far as the stabilization of h - La_2O_3 is concerned, the nature and the extension of the interface between the film and the substrate play a crucial role. Indeed, both on Si(100) and on Ge(100) a significant reactivity between the La, Si, and Ge species has been revealed and the formation of a structural and/or a chemical IL has been demonstrated. In this respect, we have systematically investigated the structural and chemical evolution of the La_2O_3 /substrate as-grown and annealed interfaces in order to unravel their repercussions on the h - La_2O_3 stabilization. On H-terminated Si(100) the use of a powerful oxidizing agent such as O_3 promotes, during the ALD growth, the formation of an amorphous SiO_x -like IL. In addition to that, Si atoms are detected by ToF SIMS also few nanometers beyond the IL, within the as-grown La_2O_3 layer. This means that, before the RTA a portion of the stack presents a silica/silicate-like composition. Upon annealing Si diffusion is further promoted through the film giving rise to the formation of a more extended interfacial region. To explain the formation of this complex interface structure we can refer to the fact that silica readily reacts with La_2O_3 forming LaSiO species.¹⁵ Regardless of the employed growth technique, LaSiO formation was indeed already reported either in as-deposited or in annealed La-based stacks.^{63,64} Since the formation of such a LaSiO region can be mainly attributed to thermodynamical factors, it can be considered independent of the total film thickness. On the contrary, the total film thickness plays a fundamental role in establishing the electrical properties of the annealed layers. In light of the observations made by XRD and ToF SIMS on films of different thickness, we can infer that the amount of $\text{La}(\text{OH})_3$ that can be actually crystallized in the h - La_2O_3 phase directly depends on the amount of Si which is present in the layer. Indeed, in thin films (<10 nm) where the Si diffusion process involves almost the full stack thickness, it is not possible to achieve a complete crystallization into the h -phase thereby promoting LaSiO formation only. A different situation is revealed in La_2O_3 /Ge stacks. HRTEM cross section does not reveal any amorphous IL; however, ToF SIMS profiles acquired on the as-grown sample suggest the presence of a chemical interfacial region in which La, Ge and O elements coexist. During ALD, the formation of La–O–Ge bondings occurs, as it has already been demonstrated in several works where La-based oxides were put directly in contact with Ge(100).^{26,28,51} Similarly to what it has been inferred for LaSiO, the formation of LaGeO is a spontaneous

reaction and does not depend on the total film thickness. The Ge atoms diffusion from the substrate is likewise promoted by the thermal treatment performed at 400 °C and consequently the chemical IL extension is increased. Given the aforementioned considerations, the issue of formation of the h - La_2O_3 crystalline phase can be more accurately discussed. We must bear in mind that LaSiO and LaGeO species cannot be reconverted into La_2O_3 by a thermal treatment but that remain stable after annealing. Therefore, only the portion of the as-grown La_2O_3 film which does not present a significant amount of Si or Ge atoms inside can be crystallized into the h -phase. Indeed, the presence of the latter elements inside the film does not allow the conversion into h - La_2O_3 .

In summary, the formation of a fairly extended LaSiO and LaGeO region at the oxide/semiconductor interface and the concomitant Si and Ge diffusion are critical in determining the possibility of generating a pure full h - La_2O_3 layer. In thin films, LaSiO(LaGeO) formation and Si(Ge) diffusion involve a considerable part of the oxide stack. Therefore, only a very limited portion of the layer can actually be converted into h - La_2O_3 . The reactivity at the interface and the atoms diffusion promoted by the thermal treatment prevent the possibility of an aggressive scaling down of the EOT thus jeopardizing the electrical performances of the whole layer. The coexistence of a LaSiO(LaGeO) interfacial region with the h - La_2O_3 phase is therefore unavoidable and has to be carefully taken into account. This leads to the definition of a so-called “critical thickness” being the minimum utilizable physical thickness of the films in order to obtain the desired dielectric response associated to the presence of h - La_2O_3 phase. Such a “critical thickness,” for as-grown films deposited using the ALD recipe discussed in this work, was found to be of the order of 20 nm on H-terminated Si(100) and 10 nm on native oxide free Ge(100). As a consequence of this, samples S5, S6, and G4 were not employed for the electrical characterization. The possibility to scale down the La_2O_3 film thickness more on Ge(100) rather than on Si(100) can be explained considering that, because of the RTA performed at lower temperature (i.e., 400 °C), the Ge atoms diffusion in annealed samples is less pronounced. However, it must be noted that the use of such an annealing temperature presents also the drawback of a fairly incomplete OH removal.

VI. CONCLUSIONS

We have deposited with ALD, using $\text{La}(\text{}^i\text{PrCp})_3$ and O_3 species, smooth, thin, and uniform La_2O_3 films on both H-terminated Si(100) and on native oxide free Ge(100) substrates at the growth temperature of 200 °C. The oxide is found amorphous in the as-deposited state. It readily reacts with moisture upon air exposure thus forming lanthanum hydroxide. However, films can be successfully converted into hexagonal h - La_2O_3 upon RTA performed in vacuum environment. Such an O_3 -based ALD process allows to obtain films in which there is no evidence of the low- k cubic La_2O_3 phase, neither before, nor after postdeposition annealing. The main aims of this work were to validate the use of O_3 as suitable oxygen source to be employed in ALD of La_2O_3 and to demonstrate the production of hexagonal h - La_2O_3 on two

different semiconductor substrates. For films grown on Si(100), after RTA performed at 600 °C in vacuum, a dielectric constant k of 24 ± 2 is obtained. Despite the amorphous SiO_x-like IL and the thermally promoted Si diffusion, which give rise to the formation of a LaSiO interfacial region, the employment of the O₃-based ALD process results in the possibility to obtain h -La₂O₃ in a 19.7 nm thick annealed film. This finding is here associated with the formation of a reasonably limited SiO_x- and LaSiO-like interfacial region. The films grown with the same ALD recipe on native oxide free Ge(100) present, after RTA in vacuum at 400 °C, a k value of 22 ± 1 . It is evidenced the presence of a LaGeO region at the interface between the semiconductor and the oxide. Although such interface reactivity limits the generation of hexagonal h -La₂O₃; a fairly high k value is demonstrated for a 6.8 nm thick annealed film. Moreover, the use of O₃ accompanied by the formation of LaGeO at the interface provides the possibility to obtain acceptably low D_{it} values.

In conclusion, an O₃-based ALD recipe has been discussed as a viable way to obtain hexagonal La₂O₃ films both on Si and on Ge. We have addressed the stabilization of the high- k hexagonal phase focusing the attention on the impact of the oxide/semiconductor interface characteristics on the overall electrical performances of the stack. These studies lead to the identification of a “critical thickness” that, although reduced, still limits an aggressive scaling down of the EOT both on Si and on Ge. However, the employment of the hexagonal La₂O₃ obtained using this ALD recipe might result in a promising solution for different stacks. The deposition of the high- k phase on alternative substrates might allow a further reduction in the total film thickness and consequently of the final EOT.

ACKNOWLEDGMENTS

This work was supported by the European FP6-Program “REALISE” (Grant No. IST-NMP 016172).

- ¹D. G. Schlom, S. Guha, and S. Datta, *MRS Bull.* **33**, 1017 (2008).
- ²B. H. Lee, S. C. Song, R. Choi, and P. Kirsch, *IEEE Trans. Electron Devices* **55**, 8 (2008).
- ³M. Bohr, R. Chau, T. Ghani, and K. Mistry, *IEEE Spectrum* **44**, 29 (2007).
- ⁴*Rare Earth Oxide Thin Films: Growth, Characterization, and Applications*, Topics in Applied Physics, edited by M. Fanciulli and G. Scarel (Springer, Berlin, 2007), Vol. 106, pp. 1–14.
- ⁵J. Robertson, *J. Appl. Phys.* **104**, 124111 (2008).
- ⁶G. Scarel, A. Debernardi, D. Tsoutsou, S. Spiga, S. C. Capelli, L. Lamagna, S. N. Volkos, M. Alia, and M. Fanciulli, *Appl. Phys. Lett.* **91**, 102901 (2007).
- ⁷D. Tsoutsou, G. Scarel, A. Debernardi, S. C. Capelli, S. N. Volkos, L. Lamagna, S. Schamm, P. E. Coulon, and M. Fanciulli, *Microelectron. Eng.* **85**, 2411 (2008).
- ⁸Y. Zhao, K. Kita, K. Kyuno, and A. Toriumi, *Appl. Phys. Lett.* **94**, 042901 (2009).
- ⁹S. Jeon and H. Hwang, *J. Appl. Phys.* **93**, 6393 (2003).
- ¹⁰M. Nieminen, M. Putkonen, and L. Niinistö, *Appl. Surf. Sci.* **174**, 155 (2001).
- ¹¹Y. Zhao, M. Toyama, K. Kita, K. Kyuno, and A. Toriumi, *Appl. Phys. Lett.* **88**, 072904 (2006).
- ¹²X. Li, D. Tsoutsou, G. Scarel, C. Wiemer, S. C. Capelli, S. N. Volkos, L. Lamagna, and M. Fanciulli, *J. Vac. Sci. Technol. A* **27**, L1 (2009).
- ¹³Y. Zhao, K. Kita, K. Kyuno, and A. Toriumi, *Jpn. J. Appl. Phys., Part 1* **46**, 4189 (2007).
- ¹⁴H. Ono and T. Katsumata, *Appl. Phys. Lett.* **78**, 1832 (2001).
- ¹⁵S. Schamm, P. E. Coulon, S. Miao, S. N. Volkos, L. H. Lu, L. Lamagna, C. Wiemer, D. Tsoutsou, G. Scarel, and M. Fanciulli, *J. Electrochem. Soc.* **156**, H1 (2009).
- ¹⁶G. Lippert, J. Dąbrowski, V. Melnik, R. Sorge, Ch. Wenger, P. Zaumseil, and H. J. Müssig, *Appl. Phys. Lett.* **86**, 042902 (2005).
- ¹⁷D. Rébiscoul, S. Favier, J. P. Barnes, J. W. Maes, and F. Martin, *Microelectron. Eng.* **87**, 278 (2010).
- ¹⁸B. H. Lee, J. Oh, H. H. Tseng, R. Jammy, and H. Huff, *Mater. Today* **9**, 32 (2006).
- ¹⁹Y. Kamata, *Mater. Today* **11**, 30 (2008).
- ²⁰J. Song, K. Kakushima, P. Ahmet, K. Tsutsui, N. Sugii, T. Hattori, and H. Iwai, *Jpn. J. Appl. Phys., Part 2* **46**, L376 (2007).
- ²¹J. Song, K. Kakushima, P. Ahmet, K. Tsutsui, N. Sugii, T. Hattori, and H. Iwai, *Microelectron. Eng.* **84**, 2336 (2007).
- ²²K. Kita, T. Takahashi, H. Nomura, S. Suzuki, T. Nishimura, and A. Toriumi, *Appl. Surf. Sci.* **254**, 6100 (2008).
- ²³J. Song, K. Kakushima, P. Ahmet, K. Tsutsui, N. Sugii, T. Hattori, and H. Iwai, *Microelectron. Eng.* **86**, 1638 (2009).
- ²⁴G. Mavrou, S. Galata, P. Tsipas, A. Sotiropoulos, Y. Panayiotatos, A. Dimoulas, E. K. Evangelou, J. W. Seo, and Ch. Dieker, *J. Appl. Phys.* **103**, 014506 (2008).
- ²⁵M. Houssa, G. Pourtois, M. Caymax, M. Meuris, and M. M. Heyns, *Appl. Phys. Lett.* **92**, 242101 (2008).
- ²⁶A. Dimoulas, D. Tsoutsou, Y. Panayiotatos, A. Sotiropoulos, G. Mavrou, S. F. Galata, and E. Golias, *Appl. Phys. Lett.* **96**, 012902 (2010).
- ²⁷V. V. Afanas'ev, A. Stesmans, G. Mavrou, and A. Dimoulas, *Appl. Phys. Lett.* **93**, 102115 (2008).
- ²⁸G. Mavrou, P. Tsipas, A. Sotiropoulos, S. F. Galata, Y. Panayiotatos, A. Dimoulas, C. Marchiori, and J. Fompeyrine, *Appl. Phys. Lett.* **93**, 212904 (2008).
- ²⁹S. F. Galata, G. Mavrou, P. Tsipas, A. Sotiropoulos, Y. Panayiotatos, and A. Dimoulas, *J. Vac. Sci. Technol. B* **27**, 246 (2009).
- ³⁰S. Abermann, O. Bethge, C. Henkel, and E. Bertagnolli, *Appl. Phys. Lett.* **94**, 262904 (2009).
- ³¹C. Andersson, C. Rossel, M. Sousa, D. J. Webb, D. Caimi, H. Siegwart, Y. Panayiotatos, A. Dimoulas, and J. Fompeyrine, *Microelectron. Eng.* **86**, 1635 (2009).
- ³²S. Guha, E. Cartier, M. A. Gribelyuk, N. A. Bojarczuk, and M. C. Copel, *Appl. Phys. Lett.* **77**, 2710 (2000).
- ³³S. Stemmer, J. P. Maria, and A. I. Kingon, *Appl. Phys. Lett.* **79**, 102 (2001).
- ³⁴T. M. Pan, C. L. Chen, W. W. Ye, and W. J. Lai, *Electrochem. Solid-State Lett.* **10**, H101 (2007).
- ³⁵S. W. Kang and S. W. Rhee, *J. Electrochem. Soc.* **149**, C345 (2002).
- ³⁶C. Bedoya, G. G. Condorelli, S. T. Finocchiaro, A. Di Mauro, D. Atanasio, I. L. Fragalà, L. Cattaneo, and S. Carella, *Chem. Vap. Deposition* **12**, 46 (2006).
- ³⁷H. Nohira, T. Shiraishi, K. Takahashi, T. Hattori, I. Kashiwagi, C. Ohshima, S. Ohmi, H. Iwai, S. Joumori, K. Nakajima, M. Suzuki, and K. Kimura, *Appl. Surf. Sci.* **234**, 493 (2004).
- ³⁸Y. H. Lin, C. H. Chien, T. Y. Yang, and T. F. Lei, *J. Electrochem. Soc.* **154**, H619 (2007).
- ³⁹H. Kim, H. B. R. Lee, and W. J. Maeng, *Thin Solid Films* **517**, 2563 (2009).
- ⁴⁰B. Y. Kim, M. G. Ko, E. J. Lee, M. S. Hong, Y. J. Jeon, and J. W. Park, *J. Korean Phys. Soc.* **49**, 1303 (2006).
- ⁴¹W. He, S. Schuetz, R. Solanki, J. Belot, and J. McAndrew, *Electrochem. Solid-State Lett.* **7**, G131 (2004).
- ⁴²D. H. Triyoso, R. I. Hedge, J. M. Grant, J. K. Schaeffer, D. Roan, B. E. White, Jr., and P. J. Tobin, *J. Vac. Sci. Technol. B* **23**, 288 (2005).
- ⁴³B. Lee, T. J. Park, A. Hande, M. J. Kim, R. M. Wallace, J. Kim, X. Liu, J. H. Yi, H. Li, M. Rousseau, D. Shenai, and J. Suydam, *Microelectron. Eng.* **86**, 1658 (2009).
- ⁴⁴J. M. Gaskell, A. C. Jones, P. R. Chalker, M. Werner, H. C. Aspinall, S. Taylor, P. Taechakumput, and P. N. Heys, *Chem. Vap. Deposition* **13**, 684 (2007).
- ⁴⁵D. Eom, S. Y. No, C. S. Hwang, and H. J. Kim, *J. Electrochem. Soc.* **154**, G49 (2007).
- ⁴⁶S. D. Elliott, G. Scarel, C. Wiemer, M. Fanciulli, and G. Pavia, *Chem. Mater.* **18**, 3764 (2006).
- ⁴⁷D. H. Triyoso, R. Gregory, M. Park, K. Wang, and S. I. Lee, *J. Electrochem. Soc.* **155**, H43 (2008).
- ⁴⁸J. Niinistö, K. Kukli, T. Sajavaara, M. Ritala, M. Leskelä, L. Oberbeck, J. Sundqvist, and U. Schröder, *Electrochem. Solid-State Lett.* **12**, G1 (2009).
- ⁴⁹D. Tsoutsou, L. Lamagna, S. N. Volkos, A. Molle, S. Baldovino, S.

- Schamm, P. E. Coulon, and M. Fanciulli, *Appl. Phys. Lett.* **94**, 053504 (2009).
- ⁵⁰A. Delabie, A. Alian, F. Bellenger, M. Caymax, T. Conard, A. Franquet, S. Sioncke, S. Van Elshocht, M. M. Heyns, and M. Meuris, *J. Electrochem. Soc.* **156**, G163 (2009).
- ⁵¹L. Lamagna, C. Wiemer, S. Baldovino, A. Molle, M. Perego, S. Schamm-Chardon, P. E. Coulon, and M. Fanciulli, *Appl. Phys. Lett.* **95**, 122902 (2009).
- ⁵²J. Kwon, M. Dai, M. D. Halls, and Y. J. Chabal, *Chem. Mater.* **20**, 3248 (2008).
- ⁵³J. B. Kim, D. R. Kwon, K. Chakrabarti, C. Lee, K. Y. Oh, and J. H. Lee, *J. Appl. Phys.* **92**, 6739 (2002).
- ⁵⁴D. Kuzum, T. Krishnamohan, A. J. Pethe, A. K. Okay, Y. Oshima, Y. Sun, J. P. McVittie, P. A. Pianetta, P. C. McIntyre, and K. C. Saraswat, *IEEE Electron Device Lett.* **29**, 328 (2008).
- ⁵⁵C. Wiemer, S. Ferrari, M. Fanciulli, G. Pavia, and L. Lutterotti, *Thin Solid Films* **450**, 134 (2004).
- ⁵⁶Inorganic Crystal Structure Database, Fachinformationszentrum, Karlsruhe, 2009, file no. 31584.
- ⁵⁷Inorganic Crystal Structure Database, Fachinformationszentrum, Karlsruhe, 2009, file no. 24693.
- ⁵⁸W. A. Hill and C. C. Coleman, *Solid-State Electron.* **23**, 987 (1980).
- ⁵⁹S. Spiga, C. Wiemer, G. Tallarida, G. Scarel, S. Ferrari, G. Seguni, and M. Fanciulli, *Appl. Phys. Lett.* **87**, 112904 (2005).
- ⁶⁰This work, that will be the subject of another publication, is on-going using systematic coupling of HRTEM to electron energy-loss spectroscopy experiments giving access to elemental profiles across interfaces.
- ⁶¹S. D. Elliott, *Surf. Coat. Technol.* **201**, 9076 (2007).
- ⁶²N. K. Park, D. K. Kang, B. H. Kim, S. J. Jo, and J. S. Ha, *Appl. Surf. Sci.* **252**, 8506 (2006).
- ⁶³J. S. Jur, D. J. Lichtenwalner, and A. I. Kingon, *Appl. Phys. Lett.* **90**, 102908 (2007).
- ⁶⁴M. Copel, E. Cartier, and F. M. Ross, *Appl. Phys. Lett.* **78**, 1607 (2001).